New Magnetically Coupled Impedance (Z-) Source Networks

Yam P. Siwakoti, *Member, IEEE*, Frede Blaabjerg, *Fellow, IEEE*, and Poh Chiang Loh

***Abstract*—Various magnetically coupled impedance source (MCIS) networks have been proposed in the literature for increasing voltage gain and modulation index simultaneously while reducing the number of passive components used in the converter. However, applications of such networks have been limited by their discontinuous currents drawn from the sources and/or high stresses experienced by their components. This paper thus proposes three new MCIS networks named, respectively, as quasi-Y-source, quasi-Γ-Z-source, and quasi-T-source or quasi-trans-Z-source networks. These new networks inherit all advantages of the existing MCIS networks. In addition, they demonstrate advantages like continuous input currents, reduced source stresses, and lower component ratings that are not achievable by other existing networks. Further, dc-current-blocking capacitors used in the networks help to avoid saturation of magnetic core. Derivations of all two-winding MCIS networks, including existing and new networks, from the generalized three-winding MCIS networks are then systematically illustrated, before comparing them. Operational principles, mathematical derivations, simulation, and experimental results of all studied networks have been presented in the paper.**

***Index Terms*—AC–AC power conversion, ac–dc power conversion, dc–ac power conversion, dc–dc power conversion, magnetically coupled impedance source (MCIS) network, Z-source network.**

I. Introduction

SINCE the publication of the first impedance (*Z*-) source network [1], various converter topologies implemented with it have gradually been reported. They overcome limitations and problems faced by the traditional voltage-source inverter (VSI), current-source inverter (CSI), as well as other classical buck–boost and unidirectional and bidirectional converters. They are, therefore, suitable for a wide range of power conversions, including dc–dc, dc–ac, ac–dc, and ac–ac conversions [2]. The major advantage of these impedance-source topologies is their flexible voltage- or current-source characteristics determined by the applications and needs under consideration. Their output voltages can also vary from 0 to theoretically ∞. They are therefore prospective topologies that can generally be represented by Fig. 1. Proper implementation of Fig. 1 will, however, require choosing the appropriate switch configuration, which, upon complemented by proper modulation and control, will reduce the number of power stages along the power conversion chain. Reliability and performance of the power electronic system can hence be improved.

Manuscript received April 20, 2015; revised June 30, 2015; accepted July 20, 2015. Date of publication July 21, 2015; date of current version June 24, 2016. Recommended for publication by Associate Editor V. P. N. Galigekere.

The authors are with the Department of Energy Technology, Aalborg University, Aalborg 9220, Denmark (e-mail: yas@et.aau.dk; fbl@et.aau.dk; pcl@et.aau.dk).

Color versions of one or more of the figures in this paper are available online at http://ieeexplore.ieee.org.

Digital Object Identifier 10.1109/TPEL.2015.2459233

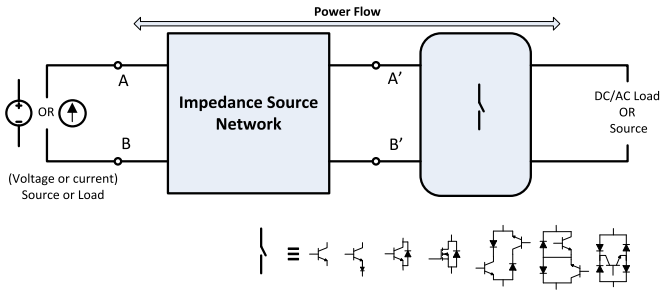

Fig. 1. General circuit configuration for illustrating impedance-source network used with different switching cells [2].

Many of the reported topologies, however, require the addition of active and passive components to their respective impedance-source networks for improving voltage gain and reducing stresses experienced by their network components [2]. They include switched-component techniques (switched inductor and switched capacitor) [3]–[5], cascading techniques (diode assisted and capacitor assisted) [6], and magnetically coupled techniques [7]. Among the three techniques, magnetically coupled techniques may be more attractive because they use lesser components and only a small shoot-through duty ratio for producing the desired high voltage gain. Shoot-through ratio here refers to the duty ratio of the switch in Fig. 1 for inserting a short circuit between nodes A' and B'. A smaller shoot-through ratio will therefore lengthen the interval for transferring energy to the load. It also permits a smaller dc-link voltage between A' and B' for producing the desired voltage across the load. Lower voltage stresses are thus experienced by the components, making magnetically coupled impedance source (MCIS) networks popular when compared with the switched-component and cascading techniques. Most MCIS networks are also observed to use only two windings including the Γ-Z-source [8], flipped-Γ-Z-source [9], T-source [10], trans-Z-source [11], TZ-source [12], LCCT-Z-source and quasi-LCCT-Z-source [13], and high-frequency-transformer-isolated Z-source [14] networks. This possibility has, however, been extended through the recent introduction of the three-winding "Y-source" network [15].

Among the winding-coupled networks, only the LCCT-Z-source and quasi-LCCT-Z-source networks draw continuous input currents from their sources. Discontinuous input currents drawn by the other networks can, at times, be problematic, especially when tied to renewable sources like photovoltaic (PV), fuel cells, and others [16]–[18]. Various techniques have therefore been reported for smoothing currents drawn from the sources like in the improved Γ-Z-source [19] and improved

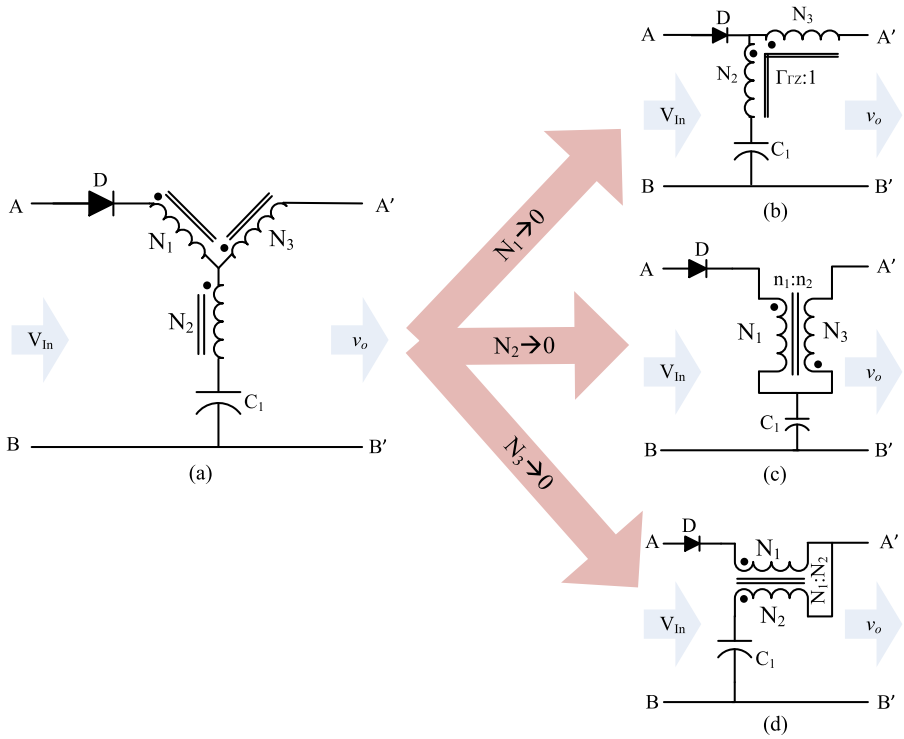

Fig. 2. Derivation of conventional two-winding MCIS networks with discontinuous input currents: (b) Γ-Z-source network, (c) T-source or trans-Z-source network, and (d) flipped Γ-source network from (a) Y-source network.

T-source or improved trans-Z-source [20] networks implemented with an additional input inductor and a capacitor. However, effects of these modifications on component stresses are often overlooked. Another approach for smoothing the input current has been explained in [13] for the T-source network with only an additional input capacitor. The modified network can indeed draw a continuous input current, but only when certain capacitance ratio is accurately set between the two capacitors used in the network. Any inaccuracy and parasitic resistances in the circuit will deteriorate the intended current smoothing. The modified network will also draw large inrush current at startup and will experience input oscillations caused by its parasitic inductances and capacitances [13].

To resolve the aforementioned concerns, three new MCIS networks are proposed in the paper, named, respectively, as the quasi-Y-source, quasi-Γ-Z-source, and quasi-T-source or quasi-trans-Z-source networks. These new networks inherit all advantages of the existing MCIS networks, in addition to drawing continuous input currents and reducing stresses shouldered by the components. Moreover, dc-blocking capacitors found in these new networks help to avoid biased magnetic core saturation, and hence, nonlinearity is unintentionally introduced to the converter. Operational principles of the networks are now studied, with the aim being to identify a generic derivative technique. The same technique can then be applied to develop various improved and quasi-MCIS networks and converters, whose features have not been previously identified. This derivation and others have been presented in Section II, before comparing the networks derived comprehensively in Section III. A single-switch dc–dc converter is then described in Section IV for evaluating each of the proposed MCIS networks. Simulation and experimental results are eventually provided in Section V for verifying the conclusion spelled in Section VI.

II. Network Derivations

The Y-source network with a three-winding coupled inductor (N_1, N_2, N_3) is shown in Fig. 2(a). Like all two-winding MCIS networks, it produces a high gain, while using only a small shoot-through duty ratio [21]. The three-winding arrangement, however, provides flexibility in choosing the winding turns ratios, which a two-winding MCIS network cannot match. The Y-source network is therefore considered as the parent MCIS network, from which other two-winding MCIS networks are derived by simply eliminating and/or rearranging the windings. Relevant derivations are provided in Sections II-A to II-C for both cases of continuous and discontinuous input currents, before their design requirements and comparison are discussed in the next section.

A. Two-Winding MCIS Networks From Y-Source Network With Discontinuous Input Current

Two-winding MCIS networks with discontinuous input currents such as the Γ-Z-source, T-source or trans-Z-source, and flipped Γ-source (or *f*Γ-Z-source in short) networks can be derived from the three-winding Y-source network by eliminating one winding and then reorientating the remaining two windings like shown in Fig. 2. For example, the T-source or trans-Z-source network can be derived from the Y-source network by eliminating winding N_2. However, it should be noted that

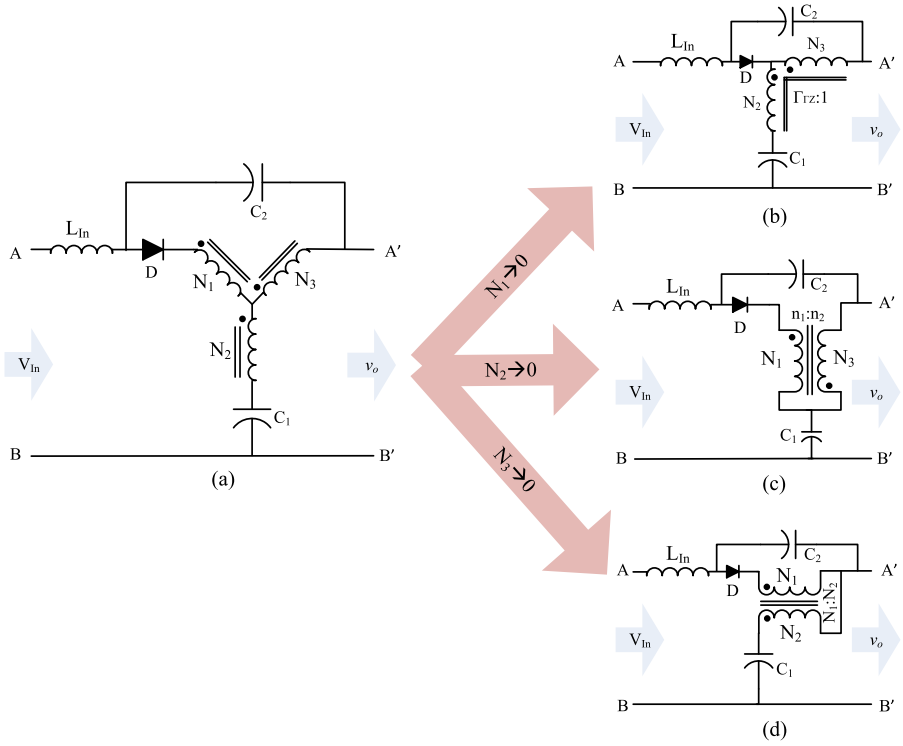

Fig. 3. Derivation of conventional Type-I two-winding improved-MCIS networks with continuous input currents: (b) improved Γ-Z-source network, (c) improved T-source or trans-Z-source network, and (d) quasi-LCCT-Z-source network from (a) improved Y-source network.

polarities of the remaining windings are not necessarily the same as the parent Y-source network. For example, in the *f*Γ-Z-source network, polarity of winding N_2 must be reversed. Despite this, design considerations and analyses of all MCIS networks with discontinuous input currents have already been discussed in the literature. They will hence not be repeated. Instead, a comparison of these MCIS networks with other derived networks drawing continuous input currents will be presented in Section III.

B. Two-Winding Improved MCIS Networks from Improved Y-Source Network with Continuous Input Current

1) Improved MCIS Networks with Continuous Input Currents: Type-I: A simple modification for smoothing the input current is presented in [19] and [20]. It involves adding an additional input capacitor and inductor, which [19] and [20] have tried with the T-source or trans-Z-source network. The same technique can be applied to the Y-source network like shown in Fig. 3(a), where the added input inductor and capacitor are notated as $L_{\rm In}$ and C_2, respectively. Winding arrangement of this new network is the same as that of the original Y-source network. Its gain is, however, increased with the same shoot-through ratio, as demonstrated later in Section III. The undesired tradeoff is higher voltage stresses across the components, as proven later. Hence, this new network may not be helpful, but can still be used for deriving different two-winding MCIS networks with continuous input currents, like presented in Section II-A.

The derived networks are shown in Fig. 3, and are respectively named as the improved Γ-Z-source, improved T-source or trans-Z-source, and quasi-LCCT-Z-source networks. Design considerations and analyses of these two-winding MCIS networks are also available in the literature, and hence, not repeated. These networks will instead be compared with other MCIS networks in Section III. From the comparison, it can be seen that all improved MCIS networks suffer from the same problem of higher component stresses when compared with those original networks drawing discontinuous input currents described in Section II-A. This is expected since they are derived from the same parent improved Y-source network.

II) Improved MCIS Networks with Continuous Input Currents: Type-II: Another simple modification for smoothing the input current is presented in [13]. It uses an additional input capacitor with the T-source or trans-Z-source network. The same technique can similarly be applied to the Y-source network like shown in Fig. 4(a). The modified network may draw a continuous input current, but only when certain capacitance ratio between C_1 and C_2 is accurately set, and parasitic resistances minimized as much as possible. The modified network also faces the risk of large inrush current at startup, and input oscillations caused by input parasitic inductances and capacitances C_1 and C_2.

Despite those and similar to the Type-I MCIS networks, different Type-II two-winding MCIS networks with continuous input currents can be derived from the new Type-II improved Y-source network. They are respectively named as the Type-II improved Γ-Z-source, improved T-source or trans-Z-source, and quasi-LCCT-Z-source networks, as shown in Fig. 4. However, due to limitations and drawbacks of the Type-II improved MCIS networks as explained earlier these topologies are not likely to have practical values and are hence not discussed further.

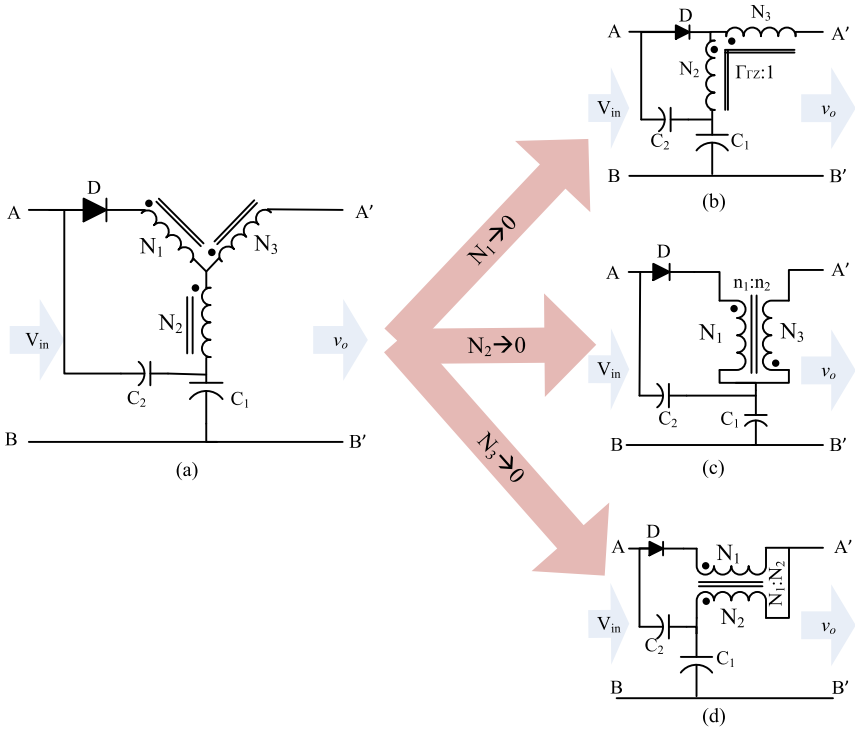

Fig. 4. Derivation of conventional Type-II two-winding improved-MCIS networks with continuous input currents: (b) improved Γ-Z-source network, (c) improved T-source or trans-Z-source network, and (d) quasi-LCCT-Z-source network from (a) improved Y-source network.

C. Two-Winding Quasi-MCIS Networks From New Quasi-Y-Source Network With Continuous Input Current

1) Quasi-Y-Source Network: A new quasi-Y-source network with continuous input current is proposed in this section as the parent network, from which various two-winding quasi-MCIS networks are derived for overcoming issues experienced by earlier described MCIS networks. The proposed network retains the three-winding coupled inductor (N_1, N_2, N_3), capacitor C_1 and their positions in the original Y-source network as shown in Fig. 2(a). The only differences here are thus an additional dc-blocking capacitor C_2 and an input inductor L_{In} used with the quasi-Y-source network in Fig. 5(a), but not the original Y-source network in Fig. 2(a). Position of diode *D* in Fig. 5(a) is also different. It is now connected between the negative terminal of C_2 and dc-link node A', as shown in Fig. 5(a).

Nonetheless, the quasi-Y-source network still operates with two operating states like all earlier mentioned MCIS networks. The first state is triggered by shorting dc-link nodes A' and B' (usually by turning on a switch), which simultaneously will cause *D* to reverse-bias like shown in Fig. 6(a). Circuit expressions during this shoot-through state can thus be written as (1) and (2), where N_1, N_2, and N_3 are the winding turns of the coupled inductor

$$V_{C_1} + \frac{N_2}{N_1}v_L - \frac{N_3}{N_1}v_L = 0 \Rightarrow v_L = \frac{N_1}{N_3 - N_2}V_{C_1} \tag{1}$$

Also

$$V_{\text{In}} - v_{L_{\text{In}}} + V_{C_2} - v_L - \frac{N_2}{N_1}v_L - V_{C_1} = 0$$

$$\Rightarrow v_{L_{\text{In}}} = V_{\text{In}} + V_{C_2} - V_{C_1} - \frac{N_1 + N_2}{N_1}v_L. \tag{2}$$

By next removing the short circuit between A' and B' (usually by turning off a switch), diode *D* conducts naturally, leading to the non-shoot-through state shown in Fig. 6(b). Circuit expressions for this state are given from (3) to (5)

$$V_{C_2} - v_L - \frac{N_3}{N_1}v_L = 0 \Rightarrow v_L = \frac{N_1}{N_1 + N_3}V_{C_2} \tag{3}$$

$$v_{L_{\text{In}}} = V_{\text{In}} + V_{C_2} - V_{C_1} - \left(\frac{N_1 + N_2}{N_1}\right)v_L \tag{4}$$

and

$$V_{\text{In}} - v_{L_{\text{In}}} - v_O = 0 \Rightarrow v_O = V_{C_1} - V_{C_2} + \left(\frac{N_1 + N_2}{N_1}\right)v_L. \tag{5}$$

Ensuring volt–sec balance between (1) and (3) then results in (6) for computing voltage ratio between C_1 and C_2, where d_{ST} represents the on-time or duty ratio of the switch for introducing the shoot-through state

$$\left(\frac{N_1}{N_3 - N_2}V_{C_1}\right)d_{ST} + \left(\frac{N_1}{N_1 + N_3}V_{C_2}\right)(1 - d_{ST}) = 0$$

$$\Rightarrow \frac{V_{C_2}}{V_{C_1}} = \frac{N_1 + N_3}{N_2 - N_3}\frac{d_{ST}}{1 - d_{ST}}. \tag{6}$$

Applying volt–sec balancing to (2) and (4) further results in (7)

$$\left\{V_{\text{In}} + V_{C_2} - V_{C_1} - \left(\frac{N_1 + N_2}{N_1}\right)v_L\right\}d_{ST}$$

$$+ \left\{V_{\text{In}} + V_{C_2} - V_{C_1} - \left(\frac{N_1 + N_2}{N_1}\right)v_L\right\}(1 - d_{ST}) = 0$$

$$\Rightarrow V_{C_1} = V_{C_2} - V_{\text{In}}. \tag{7}$$

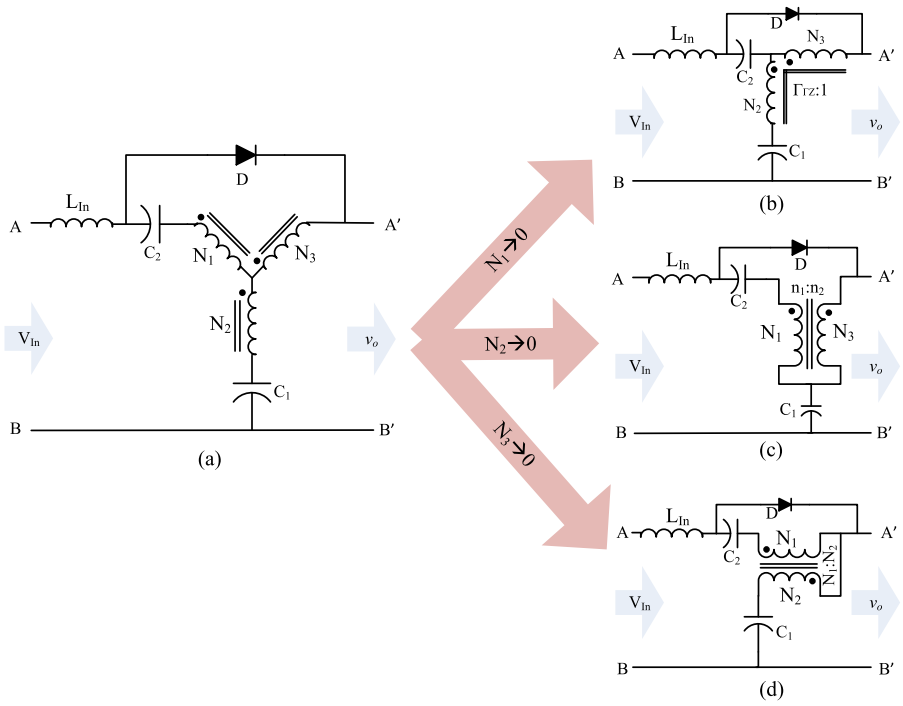

Fig. 5. Derivation of two-winding quasi-MCIS networks with continuous input currents: (b) quasi-Γ-Z-source network, (c) quasi-T-source or quasi-trans-Z-source network, and conventional (d) LCCT-Z-source network from (a) quasi-Y-source network.

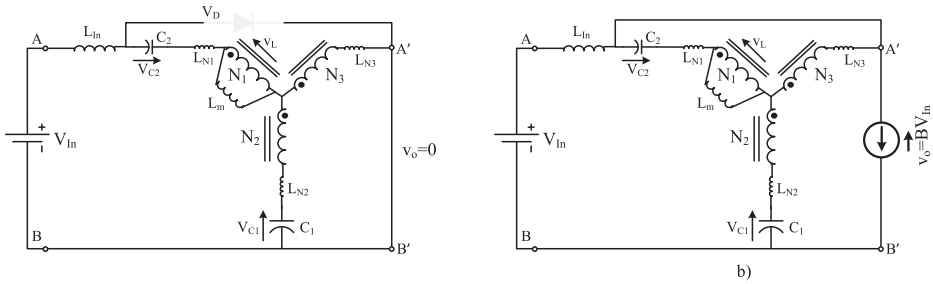

Fig. 6. Equivalent circuits of quasi-Y-source network during (a) shoot-through and (b) non-shoot-through states (leakage inductances (L_{N_1}, L_{N_2}, and L_{N_3}) and magnetizing inductance (L_m) shown are not considered for the mathematical derivation).

From (6) and (7), individual capacitor voltages can then be expressed as

$$V_{C_2} = \frac{[(N_1+N_3)/(N_2-N_3)]d_{ST}V_{\rm In}}{1-[(N_1+N_2)/(N_2-N_3)]d_{ST}}. \tag{8}$$

and

$$V_{C_1} = \frac{(1-d_{ST})V_{\rm In}}{1-[(N_1+N_2)/(N_2-N_3)]d_{ST}}. \tag{9}$$

Now, using (3), (5), (8), and (9), peak value $\hat{v}_O$ of the output voltage v_O during the non-shoot-through state can be written as (10), from which the network voltage gain $G_V = \hat{v}_O/V_{\rm In}$ can be derived in terms of the winding factor $\delta = (N_1+N_2)/(N_2-N_3)$

$$v_O = \frac{1}{1-[(N_1+N_2)/(N_2-N_3)]d_{ST}}$$
$$V_{\rm In} = \frac{1}{1-\delta d_{ST}}V_{\rm In} = BV_{\rm In} \tag{10}$$

where $B = (1/(1-\delta d_{ST}))$ is the boost factor of the quasi-Y-source impedance network. The range of d_{ST} can then be expressed as

$$0 \le d_{ST} < d_{ST,\max} = \frac{1}{\delta}. \tag{11}$$

In addition, since $V_{\rm In}I_{\rm In} = V_O I_O$ for a lossless converter, the dc input-to-output current gain can be expressed as

$$G_I = \frac{I_O}{I_{\rm In}} = 1-\delta d_{ST}. \tag{12}$$

Moreover, it is noted from (10) that winding factor of the proposed quasi-Y-source network ($\delta = (N_1+N_2)/(N_2-N_3)$) is different from that of the original Y-source impedance network ($K = (N_1+N_3)/(N_3-N_2)$) shown in Fig. 2(a). Despite that, gains of both networks are the same if their winding factors are set the same ($K = \delta$). Some possible δ values are given in Table I, together with different winding combinations that can be used for realizing them. Also given in Table I is the different gain

TABLE I
GAIN OF QUASI-Y-SOURCE IMPEDANCE NETWORK REALIZED WITH DIFFERENT WINDING FACTOR (δ) AND TURNS RATIO ($N_1 : N_2 : N_3$)

$\delta = \frac{N_1+N_2}{N_2-N_3}$	$d_{ST,\max}$	Gain G_v	$N_1 : N_2 : N_3$
2	1/2	$(1-2d_{ST})^{-1}$	(1:3:1), (2:4:1), (3:5:1)
3	1/3	$(1-3d_{ST})^{-1}$	(1:2:1), (3:3:1), (2:4:2)
4	1/4	$(1-4d_{ST})^{-1}$	(2:2:1), (1:3:2), (5:3:1)
5	1/5	$(1-5d_{ST})^{-1}$	(3:2:1), (2:3:2), (1:4:3)
6	1/6	$(1-6d_{ST})^{-1}$	(4:2:1), (3:3:2), (2:4:3)

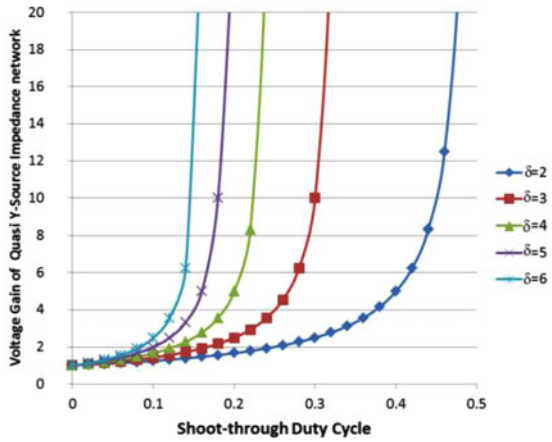

Fig. 7. Theoretical voltage gain G_v of the quasi-Y-source network obtained with different duty ratio d_{ST} and winding factor δ.

expressions for different δ, which when plotted, result in Fig. 7. Fig. 7 shows that gain of the quasi-Y-source network can be set equal or higher than that of the traditional Z-source network [1] by ensuring $\delta > 2$. This results in $1 < N_2$ and $N_2 > N_3$ as winding requirements for the proposed quasi-Y-source network, which, certainly, are different from $1 < N_3$ and $N_3 > N_2$ imposed on the original Y-source network.

Regardless of that, both Y-source networks, and in fact almost all high-boost networks, result in very steep gain curves as δ continues to increase. These steeper gain curves are generally tougher to realize because of their narrower permitted d_{ST} ranges, which will definitely require either a higher resolution or lower noise sensitivity for accurate implementation. Parameter δ should therefore not be too high in practice, even though it has no upper theoretical limit. Other advantages of the proposed quasi-Y-source network are its continuous input current and prevention of biased core saturation by its dc-blocking capacitors C_1 and C_2. These features render the network appropriate for renewable power generation systems, especially after its components are sized properly.

The sizing can conceptually begin with C_1, determined mainly by the permitted voltage ripple during shoot-through (interval $t_{\rm on}$). Assuming the permitted ripple is $\Delta V_{C_1} \le x\% \times V_{C_1}$, the following equation can be written for finding C_1:

$$C_1 = \frac{t_{\rm on}}{x\% V_{C_1}}(I_{\rm In} - I_O)$$

$$\Rightarrow C_1 = \frac{P_O}{x\% V_O^2 f_s}\frac{\delta d_{ST}^2}{(1-d_{ST})(1-\delta d_{ST})}. \quad (13)$$

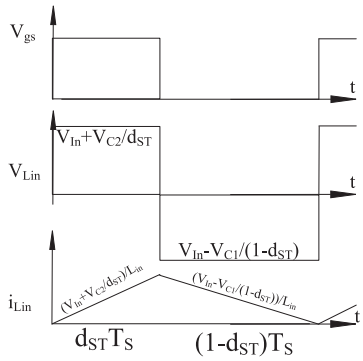

Fig. 8. Voltage and current of $L_{\rm In}$ in the quasi-Y-source network at the boundary between CCM and DCM.

Upon computing, C_1 and δ can then be substituted to (14) for determining C_2. Derivation of (14) is based on finding current expressions for the two capacitors in the shoot-through and non-shoot-through states, and then performing volt–sec balancing based on them. It should, however, be noted that C_1 and C_2 computed using (13) and (14) only give their capacitance values. Their voltage ratings must additionally be decided by considering (6), (8), and (9) derived earlier

$$C_1 = (\delta - 1)C_2. \quad (14)$$

Proceeding next to the input inductance $L_{\rm In}$, its value must be chosen such that the studied impedance network is always in the continuous conduction mode (CCM), in which all the earlier equations have been derived. Entering the discontinuous conduction mode (DCM) will invalidate most of the derived equations, and make them load dependent. It is therefore important to avoid DCM, which will occur when diode *D* in Fig. 6(b) stops conduction when in the non-shoot-through state. This can happen at light load, low switching frequency and/or small input inductance $L_{\rm In}$, and is the same discontinuous mode experienced by the first Z-source network studied in [23] and [24]. To avoid DCM, the most viable method is thus to increase $L_{\rm In}$ above a certain minimum value, since a higher switching frequency will result in higher losses, while a heavier load cannot always be guaranteed.

This minimum inductance corresponds to the boundary between CCM and DCM shown in Fig. 8. Using (1), (2), (8), and (9), voltage across $L_{\rm In}$ during the shoot-through interval notated as $d_{ST}T_s$ in Fig. 8 can then be determined as

$$V_{L_{\rm In}} = V_{\rm In} + \frac{V_{C_2}}{d_{ST}}. \quad (15)$$

Similarly, during the non-shoot-through interval notated as $(1-d_{ST})T_s$, voltage across $L_{\rm In}$ can be written as (16) after considering (3), (4), (8), and (9)

$$V_{L_{\rm In}} = V_{\rm In} + \frac{V_{C_1}}{1-d_{ST}}. \quad (16)$$

The average inductor current at the boundary can also be determined as

$$I_{\rm LB} = \frac{1}{2}\frac{V_{L_{\rm In}} t_{\rm on}}{L_{\rm In}} = \frac{1}{2}\frac{V_{L_{\rm In}} d_{ST} T_s}{L_{\rm In}}. \quad (17)$$

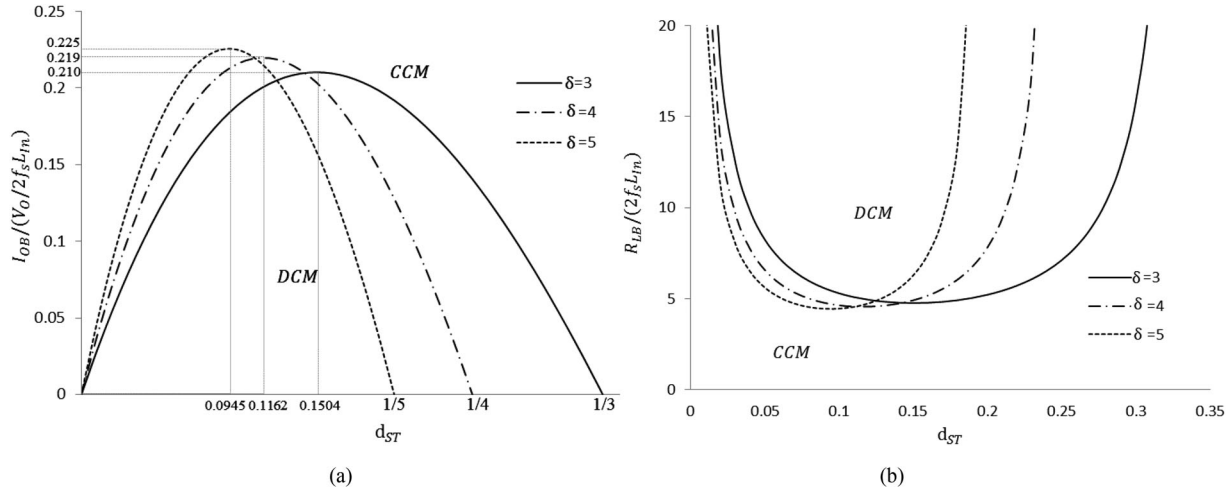

Fig. 9. Normalized (a) load current $I_{OB}/(V_O/2f_sL_{\rm In})$ and (b) load resistance $R_{LB}/(2f_sL_{\rm In})$ as functions of d_{ST} and δ.

Substituting (15) to (17) then results in

$$I_{\rm LB} = \frac{V_O}{2L_{\rm In}f_s}(1-d_{ST})\delta d_{ST}. \tag{18}$$

Further substituting (18) into (12) results in the boundary output current expressed as

$$I_{OB} = \frac{V_O}{2L_{\rm In}f_s}(1-d_{ST})(1-\delta d_{ST})\delta d_{ST}. \tag{19}$$

The largest load resistance R_{LB} that will avoid DCM is thus

$$R_{LB} = \frac{2L_{\rm In}f_s}{(1-d_{ST})(1-\delta d_{ST})\delta d_{ST}}. \tag{20}$$

From (19) and (20), Fig. 9(a) and (b) can then be plotted for showing how the normalized load current $I_{OB}/(V_O/2L_{\rm In}f_s)$ and normalized load resistance $R_{LB}/2L_{\rm In}f_s$ vary with d_{ST} and δ. Particularly, in Fig. 9(a), the peak of each curve can be determined by setting the derivative of (19) to zero, as shown

$$\frac{dI_{OB}}{dd_{ST}} = \frac{V_O}{2L_{\rm In}f_s}(3\delta^2 d_{ST}^2 - 2d_{ST}\left(\delta^2+\delta\right)+\delta = 0. \tag{21}$$

The maximum or peak I_{OB} therefore occurs when

$$d_{ST} = \frac{(\delta+1)-\sqrt{\delta^2-\delta+1}}{3\delta} = \begin{cases} 0.1504, & \text{for } \delta = 3 \\ 0.1162, & \text{for } \delta = 4 \\ 0.0945, & \text{for } \delta = 5 \end{cases}$$

which when substituted to (19), gives rise to the following maximum boundary output current:

$$I_{OB,\max} = \begin{cases} 0.2103\dfrac{V_O}{2f_sL_{\rm In,min}}, & \text{for } \delta = 3 \\ 0.2198\dfrac{V_O}{2f_sL_{\rm In,min}}, & \text{for } \delta = 4 \\ 0.2256\dfrac{V_O}{2f_sL_{\rm In,min}}, & \text{for } \delta = 5 \end{cases}. \tag{22}$$

Rearranging (22) then leads to (23) for computing the minimum input inductance needed for avoiding DCM

$$L_{\rm In} > L_{\rm In,min} = \begin{cases} 0.105\dfrac{R_L}{f_s}, & \text{for } \delta = 3 \\ 0.110\dfrac{R_L}{f_s}, & \text{for } \delta = 4 \\ 0.112\dfrac{R_L}{f_s}, & \text{for } \delta = 5 \end{cases}. \tag{23}$$

II) Quasi-Γ-Z-Source and Quasi-T-Source or Quasi-Trans-Z-Source Networks: Similar derivation like in Sections II-A and II-B can be applied to the quasi-Y-source network for deriving the quasi-Γ-Z-source network in Fig. 5(b), quasi-T-source or quasi-trans-Z-source network in Fig. 5(c), and conventional LCCT-Z-source network in Fig. 5(d). These are two-winding MCIS networks with continuous input currents. Mathematical derivations for their parameters and voltage gains are similar to those of their parent quasi-Y-source network and are hence not shown for brevity. Instead, their related expressions are listed in Table II for comparison with the other MCIS networks. In addition, it should be pointed out that for the quasi-T-source or quasi-trans-Z-source network, its design requirements are the same as those of the conventional T-source or trans-Z-source network. This is, however, not true for the quasi-Γ-Z-source network, whose new winding design requirements must satisfy $2 < N_2$ and $N_2 > N_3$, or $1 < \gamma_{q\Gamma Z} \le 2$, where $\gamma_{q\Gamma Z} = N_2/N_3$. In contrast, winding requirements of the conventional Γ-Z-source and improved Γ-Z-source networks are $2 < N_3$ and $N_3 > N_2$, or $1 < \gamma_{\Gamma Z} \le 2$, where $\gamma_{\Gamma Z} = N_3/N_2$.

To summarize, the main advantages of the newly derived quasi-MCIS networks are their continuous input currents and reduced voltage stresses, compared with their existing counterparts presented in Sections II-A and II-B. Expectations of lower voltage stresses are confirmed in Figs. 10–12 for the quasi-Y-source, quasi-Γ-Z-source, and quasi-T-source or quasi-trans-Z-source networks, respectively. These are in addition to the dc-blocking capacitors C_1 and C_2 found in the quasi-MCIS networks for preventing saturation of magnetic core. The

TABLE II
COMPARISON OF PROPOSED QUASI-MCIS NETWORKS WITH CONVENTIONAL NETWORKS

Topologies	$G_v = \hat{v}_O / V_{\rm In}$	$0 < d_{ST} < d_{ST,\max}$	V_{C_1}	V_{C_2}	V_D	$i_{\rm In}$
Y-source [see Fig. 2(a)] [15]	$[1 - K d_{ST}]^{-1}$	$0 \le d_{ST} < \frac{1}{K}$	$(1 - d_{ST}) G_v V_{\rm In}$	NA	$(K-1) G_v V_{\rm In}$	Discontinuous
Improved Y-source [see Fig. 3(a)]	$[1 - (1+K) d_{ST}]^{-1}$	$0 \le d_{ST} < \frac{1}{1+K}$	$(1 - d_{ST}) G_v V_{\rm In}$	$K d_{ST} G_v V_{\rm In}$	$(1+K) G_v V_{\rm In}$	Continuous
Quasi-Y-source [see Fig. 5(a)]	$[1 - \delta d_{ST}]^{-1}$	$0 \le d_{ST} < \frac{1}{\delta}$	$(1 - d_{ST}) G_v V_{\rm In}$	$(\delta - 1) d_{ST} G_v V_{\rm In}$	$(\delta - 1) G_v V_{\rm In}$	Continuous
Γ-Z-source [see Fig. 2(b)] [8]	$\left[1 - \frac{N_3}{N_3 - N_2} d_{ST}\right]^{-1}$	$0 \le d_{ST} < \frac{N_3 - N_2}{N_3}$	$(1 - d_{ST}) G_v V_{\rm In}$	NA	$\frac{N_2}{N_3 - N_2} G_v V_{\rm In}$	Discontinuous
Improved Γ-Z-source [see Fig. 3(b)] [19]	$\left[1 - \left(1 + \frac{N_3}{N_3 - N_2}\right) d_{ST}\right]^{-1}$	$0 \le d_{ST} < \frac{N_3 - N_2}{2N_3 - N_2}$	$(1 - d_{ST}) G_v V_{\rm In}$	$\frac{N_3}{N_3 - N_2} d_{ST} G_v V_{\rm In}$	$(1 + \frac{N_3}{N_3 - N_2}) G_v V_{\rm In}$	Continuous
Quasi-Γ-Z-source [see Fig. 5(b)]	$\left[1 - \frac{N_2}{N_2 - N_3} d_{ST}\right]^{-1}$	$0 \le d_{ST} < \frac{N_2 - N_3}{N_2}$	$(1 - d_{ST}) G_v V_{\rm In}$	$\frac{N_3}{N_2 - N_3} d_{ST} G_v V_{\rm In}$	$\frac{N_3}{N_2 - N_3} G_v V_{\rm In}$	Continuous
T-source or trans-Z-source [see Fig. 2(c)] [10], [11]	$\left[1 - \left(1 + \frac{N_1}{N_3}\right) d_{ST}\right]^{-1}$	$0 \le d_{ST} < \frac{N_3}{N_1 + N_3}$	$(1 - d_{ST}) G_v V_{\rm In}$	NA	$\frac{N_1}{N_3} G_v V_{\rm In}$	Discontinuous
Improved T-source or improved trans-Z-source [see Fig. 3(c)] [20]	$\left[1 - \left(2 + \frac{N_1}{N_3}\right) d_{ST}\right]^{-1}$	$0 \le d_{ST} < \frac{N_3}{N_1 + 2N_3}$	$(1 - d_{ST}) G_v V_{\rm In}$	$\left(1 + \frac{N_1}{N_3}\right) d_{ST} G_v V_{\rm In}$	$(2 + \frac{N_1}{N_3}) G_v V_{\rm In}$	Continuous
Quasi-T-source or quasi-trans-Z-source [see Fig. 5(c)]	$\left[1 - \frac{N_1}{N_3} d_{ST}\right]^{-1}$	$0 \le d_{ST} < \frac{N_3}{N_1}$	$(1 - d_{ST}) G_v V_{\rm In}$	$\left(\frac{N_1}{N_3} - 1\right) d_{ST} G_v V_{\rm In}$	$(\frac{N_1}{N_3} - 1) G_v V_{\rm In}$	Continuous
Flipped Γ-source [see Fig. 2(d)] [7]	$\left[1 - \frac{N_1}{N_2} d_{ST}\right]^{-1}$	$0 \le d_{ST} < \frac{N_2}{N_1}$	$(1 - d_{ST}) G_v V_{\rm In}$	NA	$(\frac{N_1}{N_2} - 1) G_v V_{\rm In}$	Discontinuous
Quasi-LCCT-Z-source [see Fig. 3(d)] [13]	$\left[1 - \left(1 + \frac{N_1}{N_2}\right) d_{ST}\right]^{-1}$	$0 \le d_{ST} < \frac{N_2}{N_1 + N_2}$	$(1 - d_{ST}) G_v V_{\rm In}$	$\frac{N_1}{N_2} d_{ST} G_v V_{\rm In}$	$(1 + \frac{N_1}{N_2}) G_v V_{\rm In}$	Continuous
LCCT-Z-source [see Fig. 5(d)] [13]	$\left[1 - \left(1 + \frac{N_1}{N_2}\right) d_{ST}\right]^{-1}$	$0 \le d_{ST} < \frac{N_2}{N_1 + N_2}$	$(1 - d_{ST}) G_v V_{\rm In}$	$\frac{N_1}{N_2} d_{ST} G_v V_{\rm In}$	$\frac{N_1}{N_2} G_v V_{\rm In}$	Continuous

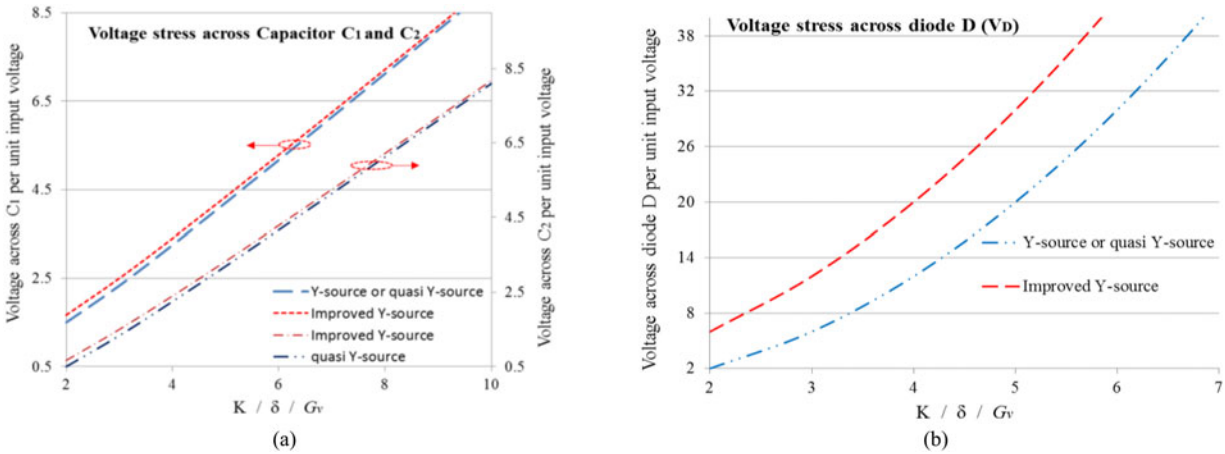

Fig. 10. Comparison of voltage stresses across (a) capacitors C_1 and C_2, and (b) diode D in the Y-source, improved Y-source, and quasi-Y-source networks under the same voltage gain G_v and winding factors $K = (N_3 + N_1)/(N_3 - N_2)$ or $\delta = (N_1 + N_2)/(N_2 - N_3)$.

quasi-method of improving MCIS networks is therefore effective, while less compromising. Similar method can also be applied to the TZ-Source and HF transformer isolated Z-source converters to obtain continuous input currents. However, the number of components especially coupled inductors increases, which to a sizable extent, makes those converters more costly and bulky. They are hence not discussed further.

III. COMPARISON OF DIFFERENT MCIS NETWORKS

Table II concisely lists governing equations of all MCIS networks for comparison. The equations are for computing dc-link voltage, input-to-output voltage gain, capacitor voltages, and reverse-blocking voltage of diode D. Also listed are the permitted range of shoot-through duty ratio and input current type (discontinuous or continuous) to better project favorable features of each new quasi-MCIS network.

Noticeably, it is seen from the table and Figs. 10–12 that voltage stresses experienced by components in the quasi-MCIS networks are either the same or lower than those of the original Y-source network. The most prominent reduction is across diode D of the quasi-T-source network, which from Fig. 12, is noted to be lower than the original T-source and improved T-source

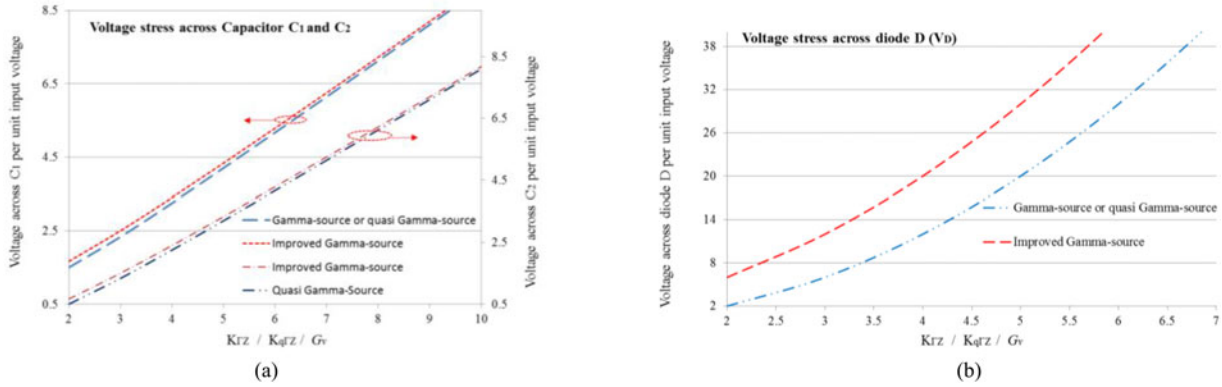

Fig. 11. Comparison of voltage stresses across (a) capacitors C_1 and C_2, and (b) diode D in the Γ-source, improved Γ-source, and quasi-Γ-source networks under the same voltage gain G_v and winding factors $K_{\Gamma Z} = N_3/(N_3 - N_2)$ or $K_{q\Gamma Z} = N_2/(N_2 - N_3)$.

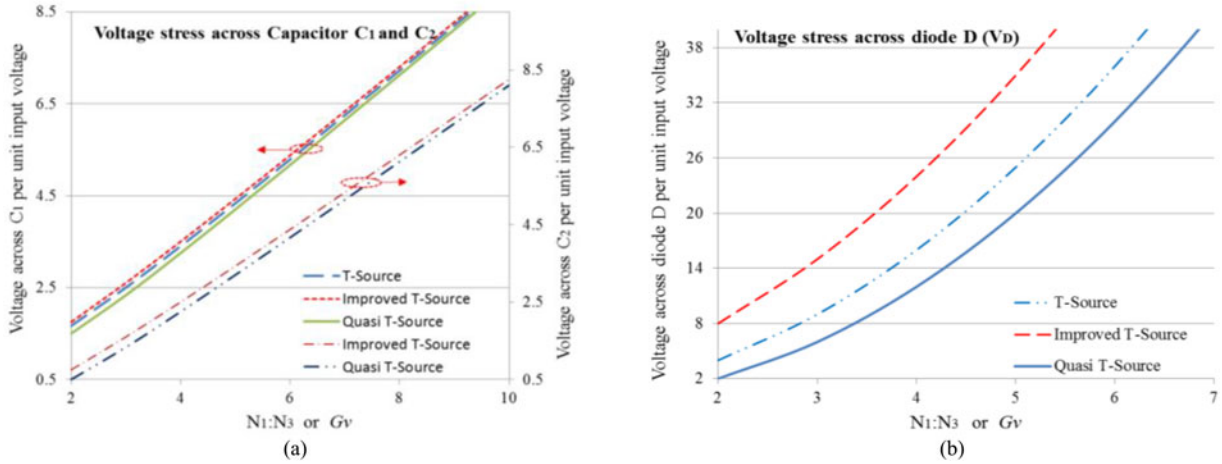

Fig. 12. Comparison of voltage stresses across (a) capacitors C_1 and C_2, and b) diode D in the T-source, improved T-source and quasi-T-source networks under the same voltage gain G_v and winding factor $N_1 : N_3$.

TABLE III
SALIENT FEATURES OF MCIS NETWORKS

Original MCIS Networks	Modified MCIS Network Topologies with Continuous Input Current		
	MCIS Networks with Existing Current Smoothing Techniques		Proposed Quasi-MCIS Networks
Fig. 2 • High voltage gain • Less components requirement • Discontinuous input current	Fig. 3 • High voltage gain • Less component requirement • Continuous input current • Higher voltage stress on components	Fig. 4 • High voltage gain • Less component requirement • Continuous input current • High inrush current • Very sensitive to ESR of capacitor and parameter variations • Unwanted resonance due to parasitic	Fig. 5 • High voltage gain • Less component requirement • Continuous input current • No inrush current • Stress on components is same or less than the original MCIS networks

networks. In contrast, voltage stresses experienced by components in the Type-I improved MCIS network are higher especially across diode *D*, which should hence be avoided where possible. The proposed quasi-MCIS networks are therefore generally more attractive than the other MCIS networks shown from Figs. 2 to 4. This is further strengthened by Table III, which summarizes salient features of each class of MCIS networks.

IV. IMPLEMENTATION OF DC–DC CONVERTER USING QUASI-MCIS NETWORK

A single-switch dc–dc converter can be implemented with the quasi-Y-source, quasi-Γ-source, or quasi-T-source, or quasi-trans-Z-source network for verifying their individual performances. Fig. 13 shows the general circuit configuration of the implemented dc–dc converter, where a switch *Q*, an additional diode D_2, and a buffer capacitor C_O have been

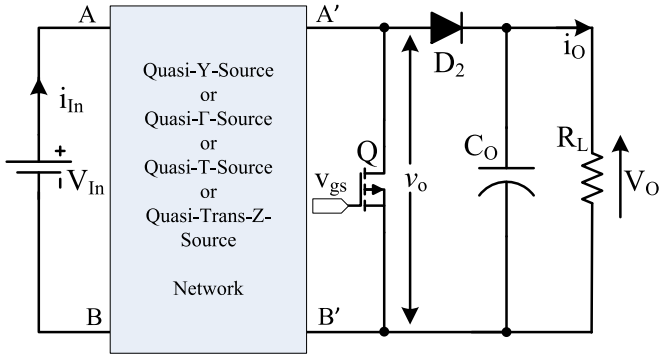

Fig. 13. Implementation of single-switch dc–dc boost converter with MCIS network.

added to the chosen impedance network. The output is then tied to a load resistor R_L with preferably ripple-free dc voltage across it. By next turning on and off switch *Q*, shoot-through and non-shoot-through states are created across nodes *A′* and *B′* of the MCIS network. Voltage across the drain–source of *Q* will then be chopping between zero and a boosted peak value $\hat{v}_O$, which is also the load voltage kept constant by C_O. Voltage gain of the converter is thus $G_v = V_O/V_{\rm In} = \hat{v}_O/V_{\rm In} = [1-\delta d_{ST}]^{-1}$, $G_v = [1-(N_2/(N_2-N_3))d_{ST}]^{-1}$, and $G_v = [1-(N_1/N_3)d_{ST}]^{-1}$ for the quasi-Y-source, quasi-Γ-source, and quasi-T-source or quasi-trans-Z-source networks, respectively, as noted from Table II.

Other waveforms expected from the dc–dc converter in Fig. 13 are shown in Fig. 14 for a given applied gate voltage v_{gs} to *Q* and input voltage $V_{\rm In}$ (respectively, first and second traces in Fig. 14). Beginning from t_0 to t_1 during which *Q* is conducting, the drain–source voltage v_O of *Q* drops to zero, while its current i_{ds} rises to a finite value. During the same time, diode *D* becomes reverse biased, allowing finite currents to flow through capacitors C_1 and C_2 in the impedance network. The input current, given by the sum of diode current and capacitor current through C_2, is thus also finite, and kept continuous by the input inductor $L_{\rm In}$. Diode *D* only resumes conduction when *Q* turns off from t_1 to t_3. During this time, diode current i_{D2} charges the buffer capacitor C_O from t_1 to t_2, while supplying the load simultaneously. Charging of C_O ends only when output voltage V_O reaches $\hat{v}_O$, and remains constant at that value until t_3. When *Q* turns on again at t_3, the waveforms repeat with the load voltage and current maintained uninterrupted, while drawing a continuous current from the source. The presented converter is thus "friendly" to the source and load, in general.

To subsequently demonstrate its efficacy, a 300-W dc–dc converter prototype has been built in the laboratory using components and parameters listed in Table IV. A picture showing the implemented converter can be found in Fig. 15, together with the three wound coupled inductors shown in Fig. 15(a) to (c) for the quasi-Y-source, quasi-Γ-source, and quasi-T-source or quasi-trans-Z-source networks. Each inductor was wound with litz wire on a Molypermalloy Powder (MPP) toroid core with 45:30:15 turns for the quasi-Y-source network, 75:50 turns for the quasi-Γ-source network, and 20:60 turns for the quasi-T-source or quasi-trans-Z-source network. Each inductor was, in

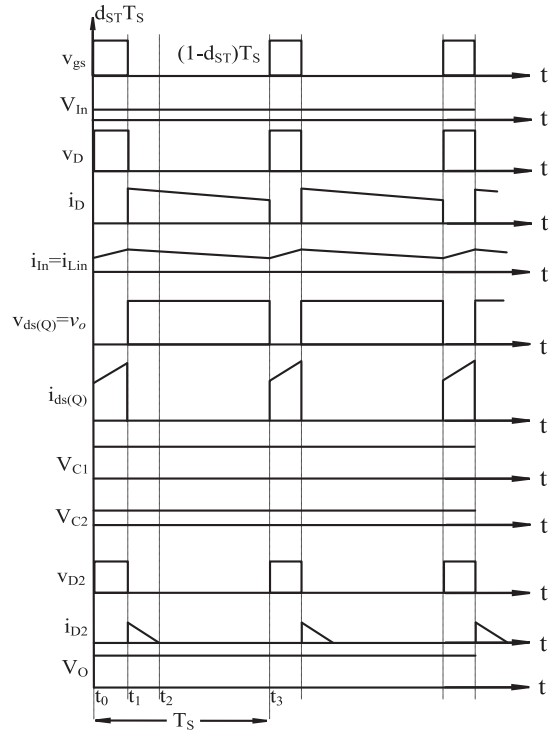

Fig. 14. Waveforms produced by single-switch dc–dc converter with quasi-MCIS network (v_{gs}, v_O, and i_{ds} → gate–source voltage, drain–source voltage and current of switch *Q*, $V_{\rm In}$, and $i_{\rm in}$ → input voltage and current, v_D and i_D → voltage and current of diode *D*, V_{C_1} and V_{C_2} → capacitor voltages, v_{D_2} and i_{D_2} → voltage and current of diode D_2, and V_O → output voltage across load).

turn, mounted on the printed circuit board for measurement with different duty ratios. The obtained results are described in the next section, together with those obtained from simulation.

V. Simulation and Experimental Results

Simulations have been carried out in MATLAB-Simulink using the PLECS toolboxes, before verifying them in experiments using the single-switch dc–dc converter prototype shown in Fig. 15. Details of the simulation and experimental results found in Figs. 16–20 are now described sequentially.

A. Quasi-Y-Source Network

Using parameters listed in Table IV, the range of duty ratio computed for the quasi-Y-source dc–dc converter with 45:30:15 turns is $0 \le d_{ST} < \frac{1}{5}$. The chosen d_{ST} value of 0.15 in Table IV is thus an acceptable value with an accompanied voltage gain of 4 according to (10). This gain is the same as that of the original Y-source converter when the same d_{ST} and winding factor of 4 are used. With an input voltage of 50 V, the theoretical output voltage will then be $V_O = 200\,\text{V}$, as also read from the third simulation and experimental traces shown in Fig. 17(a) and (b), respectively. Further, the converter draws a continuous current from the source, as seen from the second traces shown in Fig. 17(a) and (b). This is definitely different from the pulsating input current drawn by the original Y-source network, shown by the second traces plotted in Fig. 16(a) and (b). Interfacing the

TABLE IV
PARAMETERS OF QUASI-MCIS NETWORKS USED WITH SINGLE-SWITCH DC–DC CONVERTER FOR SIMULATIONS AND EXPERIMENTS

Parameter/Description		Value
Power rating (P)		300 W
Input voltage (V_{In})		50 V
Output voltage (V_O)		200 V
DC-blocking capacitors		$C_1 = 470\ \mu$F, 400 V *Kemet*
$C_2 = 150\ \mu$F, 400 V *Kemet*		
Input Inductor (L_{In})		3.5 mH
Buffer capacitor (C_O)		470 μF, 400 V *Kemet*
Switching frequency (f_s)		24.41 kHz
Shoot-through duty ratio (d_{ST})	Quasi-Y-source network	0.15
	Quasi-Γ-source network	0.25
	Quasi-T-source or quasi-trans-Z-source network	0.25
Turns ratio of coupled inductor	Quasi-Y-source network ($N_1 : N_2 : N_3$)	45:30:15 on C055710A2 core
	Quasi-Γ-source network ($N_2 : N_3$)	75:50 on C055863A2 core
	Quasi-T-source or quasi-trans-Z-source network ($N_1 : N_3$)	60:20 on C055710A2 core
Switch SW		C2M0080120D
Diode D_1		C3D25170H
Diode D_2		C3D20060D

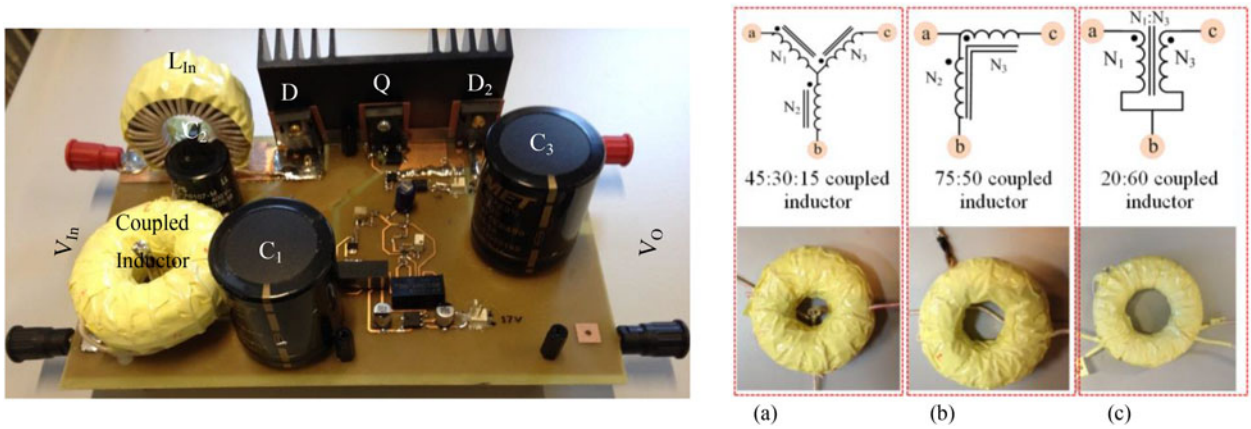

Fig. 15. Illustration of 300-W quasi-MCIS network-based dc–dc converter showing different coupled inductors (a) quasi-Y-source, (b) quasi-Γ-source, and (c) quasi-T source or quasi-trans-Z-source networks to realize a power converter.

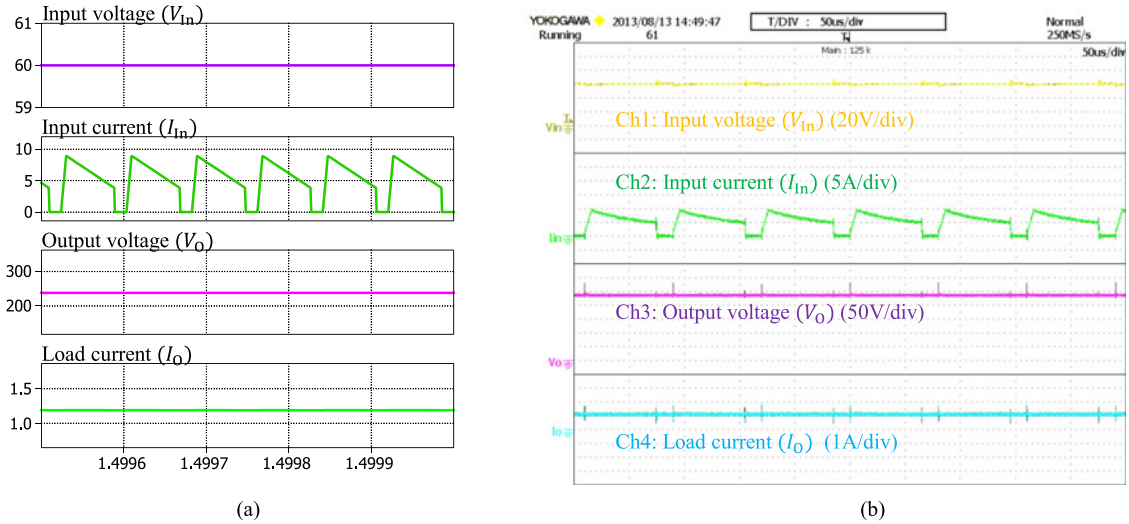

Fig. 16. Waveforms obtained from (a) simulation and (b) experiment for the Y-source boost dc–dc converter with $d_{ST} = 0.1875$, winding factor $K = 4$, and $f_s = 12.6$ kHz.

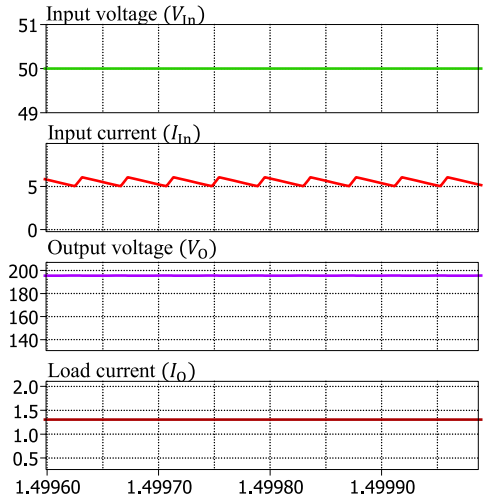

(a)

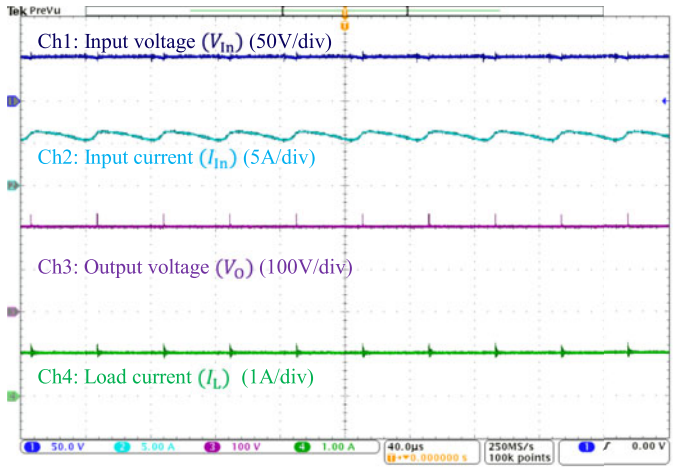

(b)

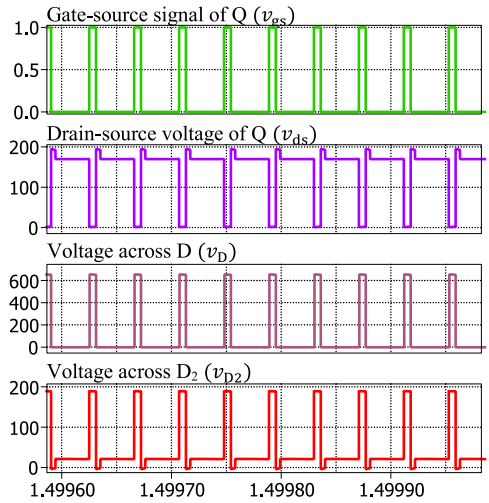

(c)

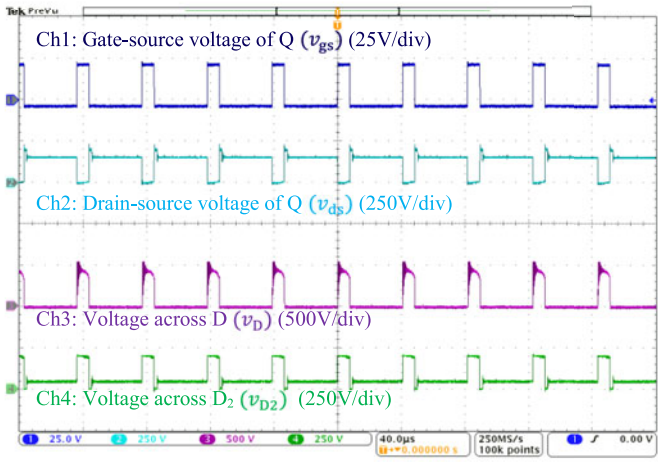

(d)

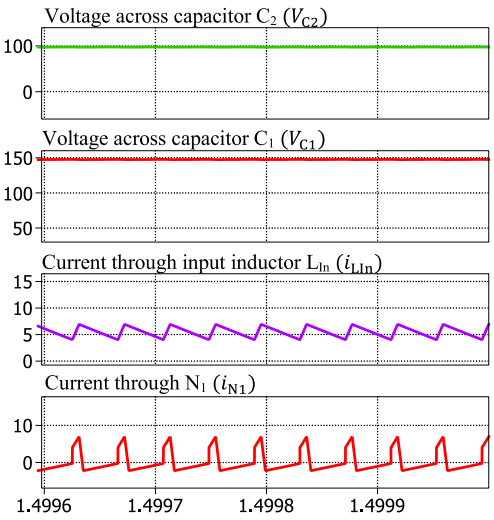

(e)

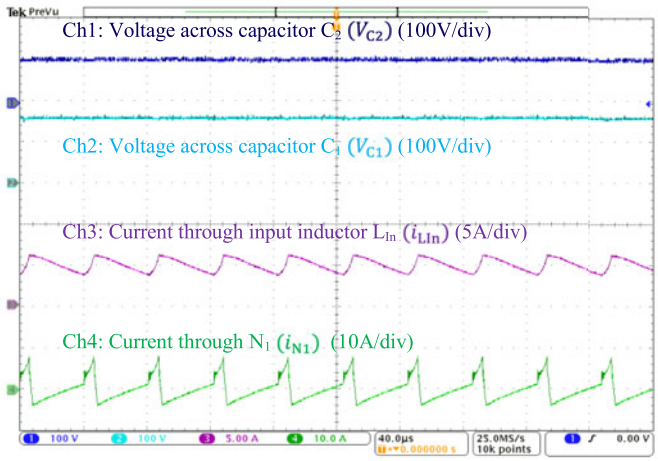

(f)

Fig. 17. Waveforms obtained from (a), (c), and (e) simulations and (b), (d), and (f) experiments for the quasi-Y-source dc–dc converter with $d_{ST} = 0.15$, winding factor $\delta = 5$, and $f_s = 24.4$kHz.

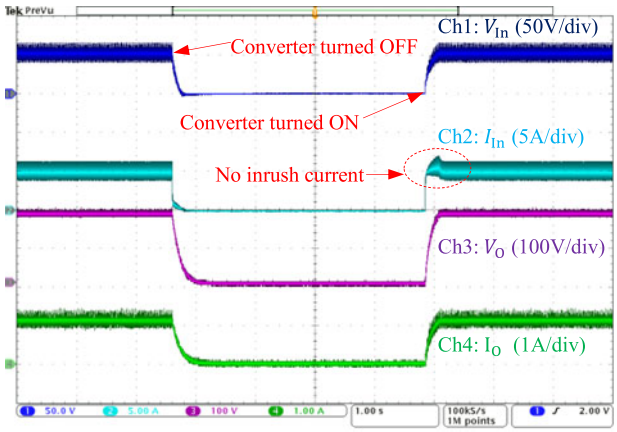

Fig. 18. Waveforms showing converter responses when input source turns on and off.

quasi-Y-source dc–dc converter to the source will therefore not cause unexpected complications.

Other waveforms showing component voltages and currents are given in Fig. 17(c) to (f). In particular, the fourth traces in Fig. 17(e) and (f) show the current through winding N_1 centered along the horizontal zero-axis. This is expected because of the dc-blocking capacitor C_2 connected in series with N_1. In addition, it should be noted from the second traces of Fig. 17(c) and (d) that the start of a non-shoot-through interval ($v_{gs} = 0$ or switch $Q \rightarrow$ off in Fig. 13) is always accompanied by a small rise in voltage v_{ds}, notated as Δv_{ds}. This voltage is contributed by the small leakage inductances of N_2 and N_3 [25], which are discharging their stored energies to capacitor C_O and load R_L in Fig. 13 over a relatively short time. Diode D_2 must therefore be conducting, as seen from its zero voltage in the fourth traces of Fig. 17(c) and (d) when $\Delta v_{ds} \neq 0$. The discharging of N_2 and N_3 (or charging of C_O) ends only when current through D_2 falls to zero, at which Δv_{ds} also falls to zero and a reverse voltage begins to appear across D_2.

Next, Fig. 18 is analyzed, where waveforms showing the turning off and then on (4.2 s later) of the quasi-Y-source converter are given. The waveforms clearly show that there is not any inrush current or oscillation, especially when the converter is turned on. Interfacing of source and load to the converter will therefore not cause unexpected complications, as mentioned earlier in Table III.

B. *Quasi-Γ-Source Network*

A coupled inductor with 75:50 turns wound on a C055863A2 MPP core is used for forming the quasi-Γ-source network. Permitted duty ratio for switch Q in Fig. 13 is then in the range of $0 \leq d_{ST} < 1/3$ according to those expressions summarized in Table II. The chosen duty ratio is thus $d_{ST} = 0.25$, which is within the range, and will give the same gain of 4 as the quasi-Y-source network. In other words, the output voltage will be $V_O = 200$ V, if the input voltage is kept at 50 V. This can clearly be seen from the third simulated and experimental traces shown in Fig. 19(a) and (b), respectively. The converter also draws a continuous current from the source, as seen from the second traces shown in Fig. 19(a) and (b). This is certainly different from the pulsating discontinuous input current drawn by the original Γ-source [8] and flipped-Γ-source [9] networks.

Other simulated and experimental waveforms shown in Fig. 19(c) to (f) are also noted to be in agreement with the theoretical values calculated using expressions listed in Table II. Performances expected from the network are thus smoothly verified. It should, however, be noted from the fourth traces of Fig. 19(e) and (f) that the slope of current i_{N1} through winding N_1 is different in both figures. This may be due to their different air-gap structures, which for the simulation, can only be performed with a concentrated air-gap and leakage flux [26]. In contrast, the experimental air-gap and leakage flux are distributed because of the powdered MPP core used for improved coupling. This difference will, however, not affect advantages expected from the quasi-Γ-source converter.

C. *Quasi-T-Source or Quasi-Trans-Z-Source Network*

The coupled inductor used for realizing quasi-T-source or quasi-trans-Z-source network has 60:20 turns wound on the same type of C055710A2 MPP core. The permitted range of duty ratio for switch Q in Fig. 13 is thus calculated as $0 \leq d_{ST} < 1/3$ using the appropriate expression found in Table II. The value eventually chosen within the range is $d_{ST} = 0.25$, which will give the same voltage gain of 4 as the other two quasi-MCIS networks. Output voltage of the converter is thus boosted to $V_O = 200$ V, if its input voltage is kept at 50 V. This can clearly be seen from the third simulated and experimental traces shown in Fig. 20(a) and (b). Simultaneously, the converter draws a continuous current from the source, as seen from the second traces shown in Fig. 20(a) and (b). It is therefore more adapting to sources unlike the discontinuous input current drawn by the original T-source or trans-Z-Source network.

Moreover, voltage stresses across capacitors C_1 and C_2 and input diode D in the quasi-T-source or quasi-trans-Z-source network are much reduced when compared with the T-source or trans-Z-source network producing the same voltage gain [10], [11]. Other simulated and measured waveforms are presented from Fig. 20(c) to (f), which are similarly in agreement with their theoretical values calculated using expressions listed in Table II. The presented results have therefore verified performances expected from the quasi-T-source or quasi-trans-Z-source network.

D. *Efficiency*

Efficiency of the dc–dc converter with each quasi-MCIS network connected is measured by varying the shoot-through or switch duty ratio from 0.05 to 0.25 for the quasi-Γ-source and quasi-T-source networks, and 0.05 to 0.15 for the quasi-Y-source network. The consolidated results are plotted in Fig. 21, where it is clear that efficiency will generally drop as the shoot-through duty ratio increases. The same trend is experienced with other existing MCIS networks and other nonmagnetically coupled boosting techniques because of the flow of larger shoot-through current when the duty ratio increases. Reducing this shoot-through current is, however, not feasible, which

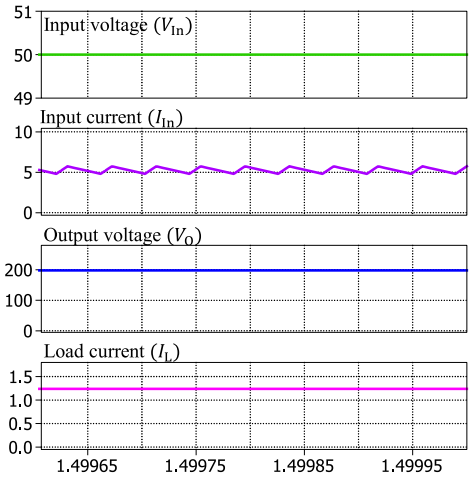

(a)

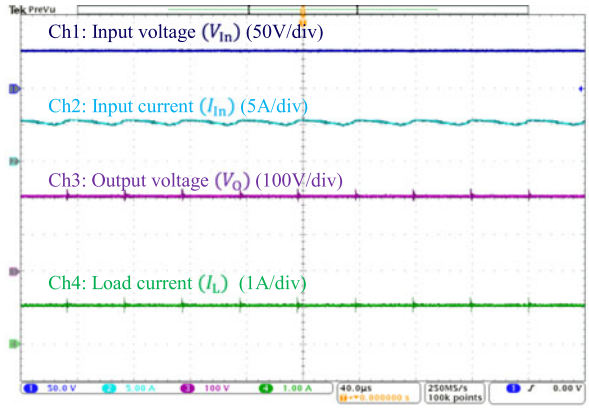

(b)

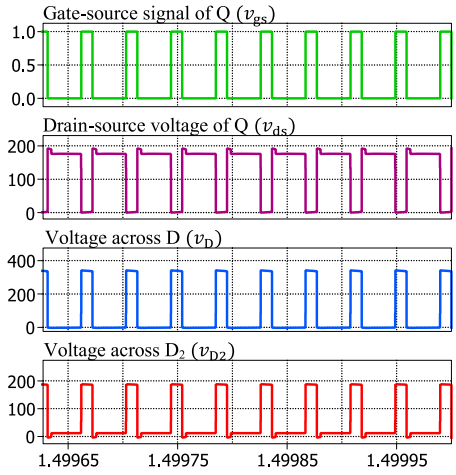

(c)

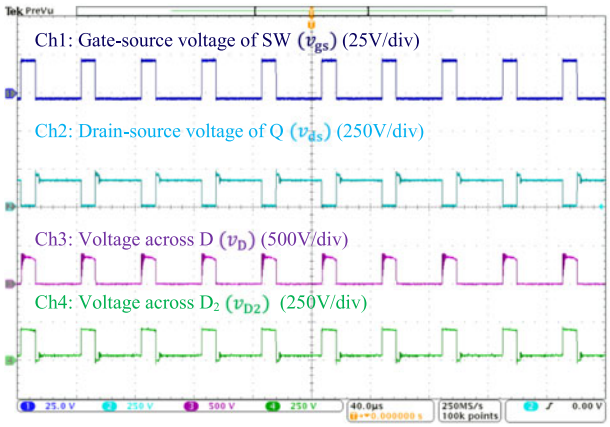

(d)

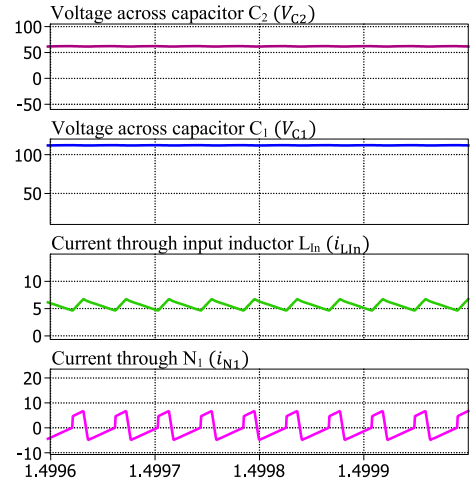

(e)

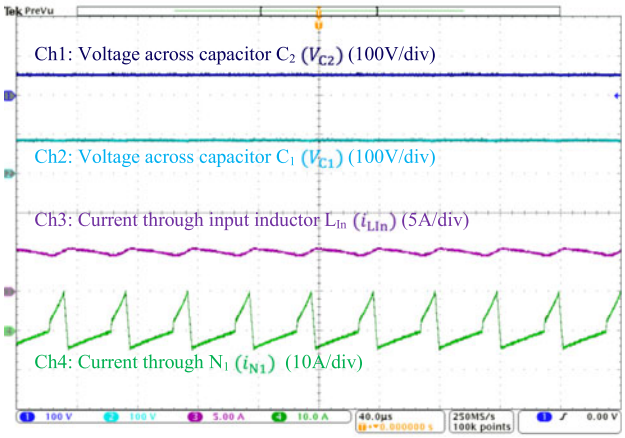

(f)

Fig. 19. Waveforms obtained from (a), (c), and (e) simulations and (b), (d), and (f) experiments for the quasi-Γ-source dc–dc converter with $d_{ST} = 0.25$, $N_2 : N_3 = 75 : 50$, and $f_s = 24.4\,\text{kHz}$.

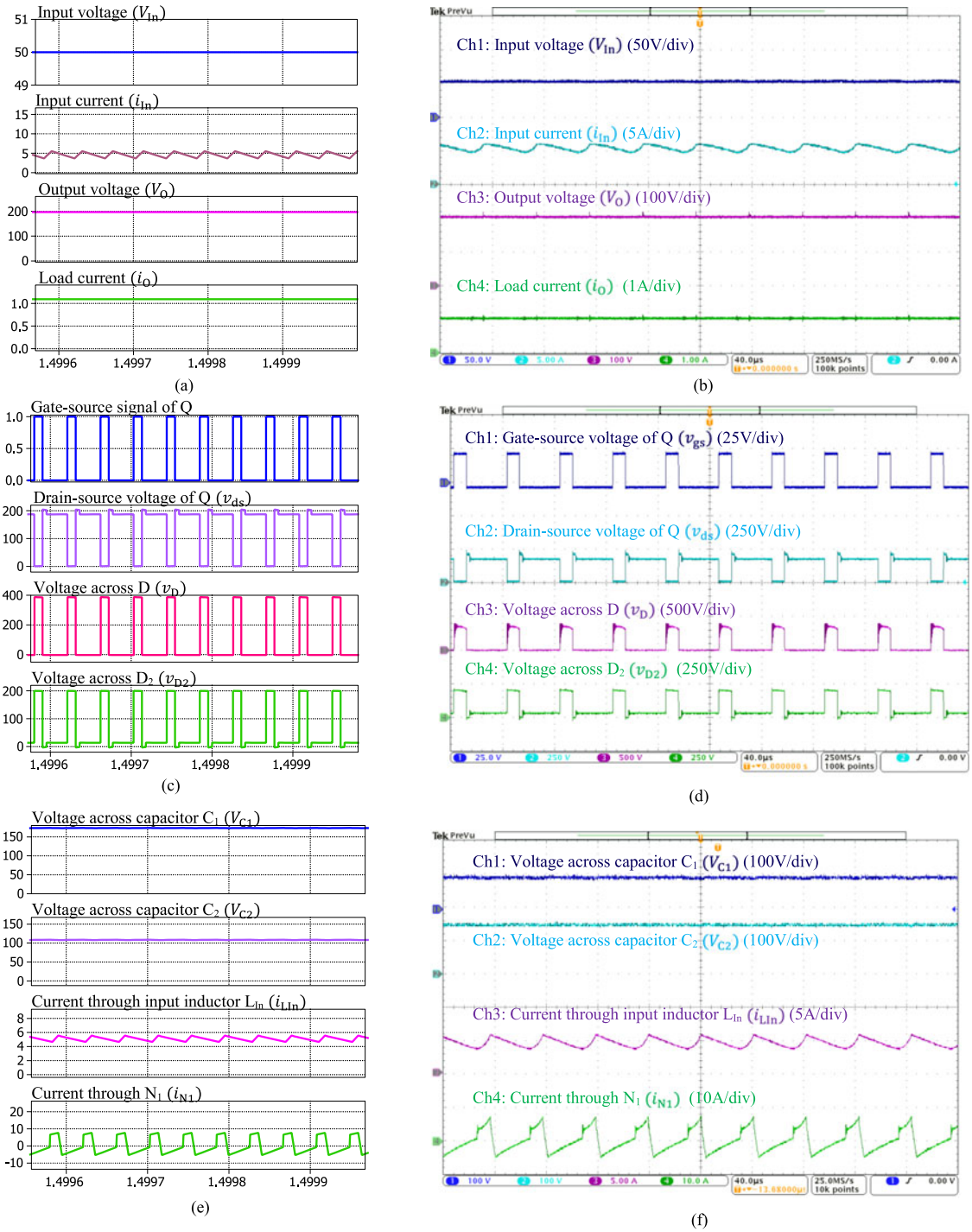

Fig. 20. Waveforms obtained from (a), (c), and (e) simulations and (b), (d), and (f) experiments for the quasi-T-source or quasi-trans-Z-source dc–dc converter with $d_{ST} = 0.25$, $N_1 : N_3 = 60 : 20$, and $f_s = 24.4\,\text{kHz}$.

means its contributed losses can only be reduced by using switches with lower $R_{DS(\text{on})}$, and better graded conductor for realizing the inductor and bus bars, especially for higher power conversion. It should, in addition, be emphasized that the 300-W dc–dc prototype has been conceived only as a proof of concept. The proposed quasi-MCIS networks can similarly be used for dc–ac, ac–dc and ac–ac conversions so long as the appropriate switch configurations [2] and modulation techniques [22] are used.

VI. Conclusion

This paper unveils three new MCIS networks, named, respectively, as the quasi-Y-source, quasi-Γ-Z-source and

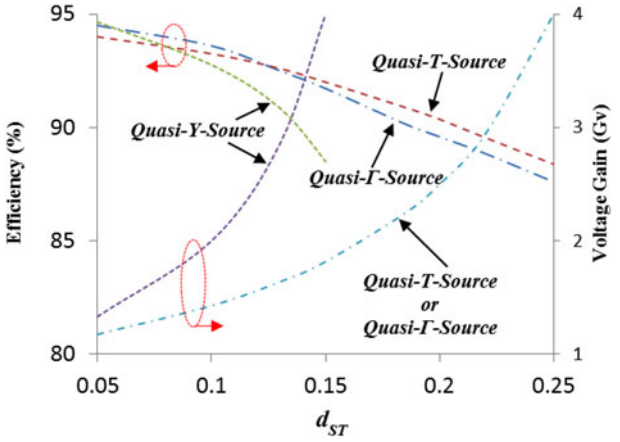

Fig. 21. Measured efficiencies and voltage gains of quasi-MCIS networks when tested with the single-switch dc–dc converter shown in Fig. 13.

quasi-T-source or quasi-trans-Z-source networks. Derivation of these quasi-MCIS and other conventional networks from their respective parent three-winding Y-source networks has been illustrated, before comparing them comprehensively. The comparison shows that the proposed MCIS networks inherit all advantages of the conventional MCIS networks including a very high boost capability and flexibility in design because of the presence of multiple circuit parameters for gain tuning. Other advantages of the quasi-MCIS networks include their continuous input currents, reduced source stresses, and lower component ratings when compared with their conventional counterparts. In addition, dc-blocking capacitors found in the new networks prevent biased saturation of the magnetic core caused by dc current. These advantages and feasibility of the proposed quasi-MCIS networks have been validated by both simulation and experimental results obtained with an example single-switch dc–dc converter.

REFERENCES

[1] F. Z. Peng, "Z-source inverter," in *Proc. Ind. Appl. Conf.*, Oct. 13–18, 2002, vol. 2, pp. 775–781.
[2] Y. P. Siwakoti, F. Z. Peng, F. Blaabjerg, P. C. Loh, and G. E. Town, "Impedance source network for electric power conversion—Part I: A topological review" *IEEE Trans. Power Electron.*, vol. 30, no. 2, pp. 699–716, Feb. 2015.
[3] M. Zhu, K. Yu, and F. L. Luo, "Switched inductor Z-source inverter," *IEEE Trans. Power Electron.*, vol. 25, no. 8, pp. 2150–2158, Aug. 2010.
[4] D. Li, P. C. Loh, M. Zhu, F. Gao, and F. Blaabjerg, "Generalised multicell switched-inductor and switched-capacitor Z-source inverters," *IEEE Trans. Power Electron.*, vol. 28, no. 2, pp. 837–848, Feb. 2013.
[5] M. K. Nguyen, Y. C. Lim, and G. B. Cho, "Switched-inductor quasi-Z-source inverter," *IEEE Trans. Power Electron.*, vol. 26, no. 11, pp. 3183–3191, Nov. 2011.
[6] C. J. Gajanayake, F. L. Luo, H. B. Gooi, P. L. So, and L. K. Siow, "Extended-boost Z-source inverters," *IEEE Trans. Power Electron.*, vol. 25, no. 10, pp. 2642–2652, Oct. 2010.
[7] P. C. Loh and F. Blaabjerg, "Magnetically coupled impedance-source inverters," *IEEE Trans. Power Electron.*, vol. 49, no. 5, pp. 2177–2187, Sep./Oct. 2013.
[8] P. C. Loh, D. Li, and F. Blaabjerg, "Γ-Z-source inverters," *IEEE Trans. Power Electron. (Lett.)*, vol. 28, no. 11, pp. 4880–4884, Nov. 2013.
[9] P. C. Loh and F. Blaabjerg, "Magnetically coupled impedance-source inverters," *IEEE Trans. Power Electron.*, vol. 49, no. 5, pp. 2177–2187, Sep./Oct. 2013.
[10] R. Strzelecki, M. Adamowicz, N. Strzelecka, and W. Bury, "New type T-source inverter," in *Proc. CPE 2009*, May 2009, pp. 191–195.
[11] W. Qian, F. Z. Peng, and H. Cha, "Trans-Z-source inverters," *IEEE Trans. Power Electron.*, vol. 26, no. 12, pp. 3453–3463, Dec. 2011.
[12] M. K. Nguyen, Y. C. Lim, and Y. G. Kim, "TZ-source inverters," *IEEE Trans. Ind. Electron.*, vol. 60, no. 12, pp. 5686–5695, Dec. 2013.
[13] M. Adamowicz, R. Strzelecki, F. Z. Peng, J. Guzinski, and A. H. Rub, "New type LCCT-Z-source inverters," in *Proc. EPE*, Sep. 2011, pp. 1–10.
[14] S. Jiang, D. Cao, and F. Z. Peng, "High frequency transformer isolated Z-source inverters," in *Proc. APEC*, Mar. 2011, pp. 442–449.
[15] Y. P. Siwakoti, P. C. Loh, F. Blaabjerg, and G. E. Town, "Y-source inverter" in *Proc. IEEE PEDG*, Jun. 2014, pp. 1–6.
[16] B. Williams, "DC-to-DC converters with continuous input and output power," *IEEE Trans. Power Electron.*, vol. 28, no. 5, pp. 2307–2316, May 2013.
[17] A. H. El Khateb, N. A. Rahim, J. Selvaraj, and B. W. Williams, "DC-to-DC converter with low input current ripple for maximum photovoltaic power extraction," *IEEE Trans. Ind. Electron.*, vol. 62, no. 4, pp. 2246–2256, Apr. 2015.
[18] C. Liu and J. S. Lai, "Low frequency current ripple reduction technique with active control in a fuel cell power system with inverter load," *IEEE Trans. Power Electron.*, vol. 22, no. 4, pp. 1429–1436, Jul. 2007.
[19] W. Mo, P. C. Loh, and F. Blaabjerg, "Asymmetrical Ã-source inverters," *IEEE Trans. Ind. Electron.*, vol. 61, no. 2, pp. 637–647, Feb. 2014.
[20] M. K. Nguyen, Y. C. Lim, and S. J. Park, "Improved trans-Z-source inverter with continuous input current and boost inversion capability," *IEEE Trans. Power Electron.*, vol. 28, no. 10, pp. 4500–4510, Oct. 2013.
[21] Y. P. Siwakoti, P. C. Loh, F. Blaabjerg, S. J. Andreasen, and G. E. Town, "Y-source impedance network based boost DC/DC converter for distributed generation," *IEEE Trans. Ind. Electron.*, vol. 62, no. 2, pp. 1059–1069, Feb. 2015.
[22] Y. P. Siwakoti, F. Z. Peng, F. Blaabjerg, P. C. Loh, G. E. Town, and S. Yang, "Impedance source network for electric power conversion—Part II: Review of control and modulation techniques," *IEEE Trans. Power Electron.*, vol. 30, no. 4, pp. 1887–1905, Apr. 2015.
[23] M. Shen and F. Z. Peng, "Operation modes and characteristics of the Z-source inverter with small inductance or low power factor," *IEEE Trans. Ind. Electron.*, vol. 55, no. 1, pp. 89–96, Jan. 2008.
[24] V. P. Galigekere and M. K. Kazimierczuk, "Analysis of PWM Z-source DC–DC converter in CCM for steady state," *IEEE Trans. Circuits Syst.*, vol. 59, no. 4, pp. 854–863, Apr. 2012.
[25] Y. P. Siwakoti, P. C. Loh, F. Blaabjerg, and G. E. Town, "Effects of leakage inductances on magnetically-coupled impedance-source networks" *IEEE Trans. Power Electron. (Lett.)*, vol. 29, no. 11, pp. 5662–5666, Nov. 2014.
[26] (2015, Jun. 20). [Online]. Available: http://www.plexim.com/support/application-examples/186

Yam P. Siwakoti (S'10–M'14) received the B.Tech. degree in electrical engineering from NIT Hamirpur, Hamirpur, India, in 2005, the M.E. degree in electrical power engineering (*magna cum laude*) from Norwegian University of Science and Technology (NTNU), Trondheim, Norway, and Kathmandu University, Kathmandu, Nepal, in 2010, and the Ph.D. degree from Macquarie University, Sydney, NSW, Australia, in 2014.

He is currently a Postdoctoral Researcher in the Department of Energy Technology, Aalborg University, Aalborg, Denmark. His current research interests include modeling and design of high power density converter; investigate new power converter topology with higher efficiency, reliability and power density; application of new wide-band-gap semiconductor devices (GaN/SiC) for VHF power converter, and wireless power transfer. He has authored or coauthored more than 30 research papers in refereed journals and conference proceedings in the area of power electronics.

Dr. Siwakoti is an Associate Editor (Guest) of the IEEE TRANSACTION ON POWER ELECTRONICS SPECIAL ISSUES ON THE IMPEDANCE SOURCE CONVERTER TOPOLOGIES AND APPLICATIONS. He is also a frequent reviewer of APEC2013, IECON2013 and APEC2014 conferences and the IEEE TRANSACTION ON INDUSTRIAL ELECTRONICS, the IEEE TRANSACTION ON POWER ELECTRONICS, the IEEE TRANSACTION ON INDUSTRY APPLICATION, the IEEE TRANSACTION ON INDUSTRIAL INFORMATICS, the IEEE INTERNATIONAL JOURNAL OF CIRCUIT THEORY AND APPLICATIONS, the *IET Power Electronics*, and the *IET Renewable Power Generation*.

Frede Blaabjerg (S'86–M'88–SM'97–F'03) received the Ph.D. degree from Aalborg University, Aalborg, Denmark, in 1992.

He was with ABB-Scandia, Randers, Denmark, from 1987 to 1988. He became an Assistant Professor in 1992, an Associate Professor in 1996, and a Full Professor of power electronics and drives in 1998 at Aalborg University. His current research interests include power electronics and its applications such as in wind turbines, PV systems, reliability, harmonics, and adjustable speed drives.

Dr. Blaabjerg received 15 IEEE Prize Paper Awards, the IEEE PELS Distinguished Service Award in 2009, the EPE-PEMC Council Award in 2010 and the IEEE William E. Newell Power Electronics Award 2014. He was an Editor-in-Chief of the IEEE TRANSACTIONS ON POWER ELECTRONICS from 2006 to 2012. He has been a Distinguished Lecturer for the IEEE Power Electronics Society from 2005 to 2007 and for the IEEE Industry Applications Society from 2010 to 2011.

Poh Chiang Loh received the B.Eng. (Hons.) degree and the M.Eng. from the National University of Singapore, Singapore. Singapore, in 1998 and 2000, respectively, and the Ph.D. degree from Monash University, Australia, in 2002, all in electrical engineering.

Since 2013, he has been with Aalborg University, Aalborg, Denmark.